Desalination and Water Treatment
www.deswater.com

doi: 10.5004/dwt.2020.25927

196 (2020) 146–160
August

Efficient simultaneous removal of anionic phosphate and cationic ammonium using amphoteric cellulose/laponite nanocomposite hydrogel

Yin Wang, Ruotong Wang, Lan Yu, Yun Wang, Xiaodong Zhang*

School of Environment and Architecture, University of Shanghai for Science and Technology, Shanghai 200093, China, emails: fatzhxd@126.com (X.D. Zhang), 625xiaogui@163.com (Y. Wang), 877524165@qq.com (R. Wang), 1484846156@qq.com (L. Yu), 1483247383@qq.com (Y. Wang)

Received 14 October 2019; Accepted 4 April 2020

ABSTRACT

Amphoteric cellulose/laponite nanocomposite hydrogel (AC/Lap-Hy) was successfully synthesized by using dodecyl dimethyl betaine (BS-12) as a zwitterionic modifier and Laponite as a physical crosslinker and applied simultaneously to remove cationic ammonium and anionic phosphate from water. The characteristics of AC/Lap-Hy indicated that the required binding sites were successfully grafted onto the hydrogel and the porous structure was formed. Batch adsorption experiment showed that the maximum adsorption capacity for phosphate and ammonium was at pH 6.0 and 8.0, respectively. The adsorption isotherm and kinetic could be well described by Langmuir and the pseudo-second-order model. Furthermore, the adsorption of phosphate was endothermic, while exothermic for ammonium. AC/Lap-Hy could be regenerated effectively and recycled. Moreover, the adsorption mechanism was possible dominated by chemisorption. These superior properties of AC/Lap-Hy demonstrated it as a promising adsorbent in the simultaneous treatment of wastewaters containing both ammonium and phosphate.

Keywords: Amphoteric modification; Nanocomposite hydrogel; Ammonium; Phosphate; Adsorption mechanism

1. Introduction

In many countries, eutrophication is the major water pollution problem which leads to the depletion of dissolved oxygen and has a deleterious effect on fish and aquatic lives [1]. The combined action of inorganic nitrogen and phosphorus such as nitrate, ammonium, and phosphate are the main factor contributing to water eutrophication, whereas the coexistence of ammonium and phosphate have a more significant impact on living organisms [2]. As various treatment technologies can be used in water pollution treatment [3–5], technologies such as precipitation, crystallization, biological removal, adsorption, and ion exchange have been developed for removing ammonium and phosphate [6]. Among which, adsorption is superiority to other techniques in the aspects of economic feasibility and environmentally friendly behavior [7].

Lately, three-dimensional crosslinked hydrogel has been widely used in the adsorption of heavy metals [8], dyes [9], and ammonium [10] because of its high absorptivity, reusability, and operability. Furthermore, there has been increased concern in preparing bio-hydrogels by using natural biomass materials such as cellulose and its derivatives, which exhibit the properties of environmentally friendly, biocompatibility, degradability, and rich sources. And they have been used as raw materials to synthesize bio-hydrogels, such as cellulose/gelatin composite hydrogel [11], aminated hyaluronic acid/oxidized hydroxyethyl cellulose hydrogel [12], cellulose/phenylboronic acid composite intelligent bio-hydrogel [13], and potassium copper

* Corresponding author.

hexacyanoferrate-cellulose hydrogel [14], which show high biocompatibility and affinity to many kinds of cationic pollutants.

However, there are also some shortcomings for the bio-hydrogels such as low mechanical strength and slow reaction rate. Several studies have reported that introducing of layered silicate nano-clay into polymer matrix to fabricate nanocomposite hydrogels could overcome these deficiencies [15]. Laponite (Lap), a type of synthetic layered nano silicate clay has two kinds of charges (positive charge and negative charge) both in its interlayer and on its surface. These charges are favorable for the interaction with cationic, anionic, and neutral polymers to form a physical interconnection network architecture with spatial homogeneity characteristic [16]. Li et al. [17] synthetized a nanocomposite hydrogel consisting of N-isopropylacrylamide and Laponite. The Laponite was modified and used as the physical crosslinker, which greatly improved the mechanical strength of the hydrogel. However, the strong negative charges of Laponite will lead to an extremely low adsorption capacity toward anionic pollutants [18], which brings challenge for phosphate adsorption in eutrophic water. As a result, it is necessary to develop amphoteric hydrogel for simultaneous removal of anionic phosphate and cationic ammonium.

Recently, cationic and anionic monomers are recognized as one of the most promising candidates for the preparation of amphoteric hydrogels [19]. The amphoteric hydrogels which contain both negatively and positively charged groups could interact with cationic and anionic pollutants, respectively, by electrostatic attraction [20]. Lin et al. [21] synthesized amphoteric polymer adsorbent by using carboxymethyl cellulose as raw material, and crosslinking with monochloroacetic acid modified epichlorohydrin, which showed excellent removal performance toward methylene blue (cationic) and orange II (anionic) dyes. Similarly, amphoteric nanocomposite hydrogel was successfully prepared by using N-[3-(dimethylamino)propyl] methacrylamide as cationic monomer and acrylic acid (AA) as anionic monomer by Nie et al. [22].

Despite the successful preparation of above hydrogels that were modified by cationic and anionic monomers, few studies have focused on the production of amphoteric hydrogel using zwitterionic surfactants as modifiers. Betaine, containing both positively charged (quaternary ammonium) and negatively charged (carboxyl) groups is an example of zwitterionic surfactant, which can retain the zwitterionic characteristic over a broad pH range [23]. Besides, the presence of betaine could endow the nanocomposite hydrogel distinctive electrochemical properties and promote the interaction between surfactants and Lap [24]. As a result, the amphoteric nanocomposite hydrogel might be expected to simultaneously remove phosphate and ammonium in one step.

In this study, a versatile cellulose based amphoteric nanocomposite hydrogel (AC/Lap-Hy) was successfully synthesized according to free radical copolymerization by using dodecyl dimethyl betaine (BS-12) as zwitterionic monomer and laponite (Lap) as physical crosslinker. The physicochemical properties of AC/Lap-Hy were examined by scanning electron microscopy (SEM), X-ray diffraction (XRD), Fourier transform infrared spectroscopy (FTIR), and thermogravimetry (TG) characterization. Adsorption properties for phosphate and ammonium in both single and binary system were investigated. Furthermore, the adsorption mechanism of AC/Lap-Hy was elucidated systematically.

2. Materials and methods

2.1. Reagents

Microcrystalline cellulose (MCC), N,N,N′,N′-tetramethylethylenediamine (TEMED), potassium peroxydisulfate (KPS), dodecyl dimethyl betaine (BS-12), ammonium chloride (NH_4Cl), potassium dihydrogen phosphate (NaH_2PO_4) were obtained from Sinopharm Chemical Reagent Co., Ltd., (China), Laponite (Lap), a particular gel-forming grade, was purchased from Rockwood Co., U.S. All chemical reagents were of analytical grade and used without further purification.

2.2. Synthesis of AC/Lap-Hy, C/Lap-Hy, and C-Hy

Amphoteric cellulose/laponite nanocomposite hydrogel (AC/Lap-Hy) was fabricated via free-radical polymerization. MCC was used as raw material which was firstly dissolved in the NaOH/urea/H_2O (wt.% = 7:12:81) solvent after freezing for 12 h in a refrigerator (–5°C to –10°C), and then thawed to get the homogeneous cellulose solution (wt.% = 3%). Then, cellulose solution (10 mL) was mixed with BS-12 (0.02 mol) and Lap (0.3 g). After stirring in an ice bath for about 2 h, catalyst TEMED (20 μL) and initiator KPS (0.15 g) were added with stirring in a water bath at 20°C for 24 h to finish the free-radical polymerization. At last, the product was washed with deionized water for several times to remove excessive agents and freeze-dried for 48 h. The schematic diagram for preparation of AC/Lap-Hy was showed in Fig. 1.

Lap nanocomposite hybrid cellulose hydrogel (C/Lap-Hy) was synthesized by mixing cellulose solution (10 mL) with Lap (0.3 g), followed by stirring in ice bath for 2 h. Then free-radical polymerizing with catalyst TEMED (20 μL) and initiator KPS (0.15 g), and stirring in water bath at 20°C for 24 h. The product was finally obtained after washing with deionized water and freeze-drying for 48 h.

The bulk cellulose hydrogel (C-Hy) was fabricated according to the traditional method by simply mixing cellulose solution (10 mL) with initiator KPS (0.15 g) and chemical crosslinker MBA (0.05 g), and then free-radical polymerizing in water bath at 20°C for stirring continuously for 24 h. At last, washed with deionized water and freeze-dried for 48 h.

2.3. Material characterization

Surface morphologies of the materials were examined on an SEM (Hitachi S-4800, Japan) after sputter coating with gold under vacuum. Surface area and pore-size distribution of the as-prepared hydrogels were measured by N_2 adsorption–desorption instrument (BET, Quantachrome autosorb-iQ-2MP, USA). FTIR spectra of the samples were recorded on

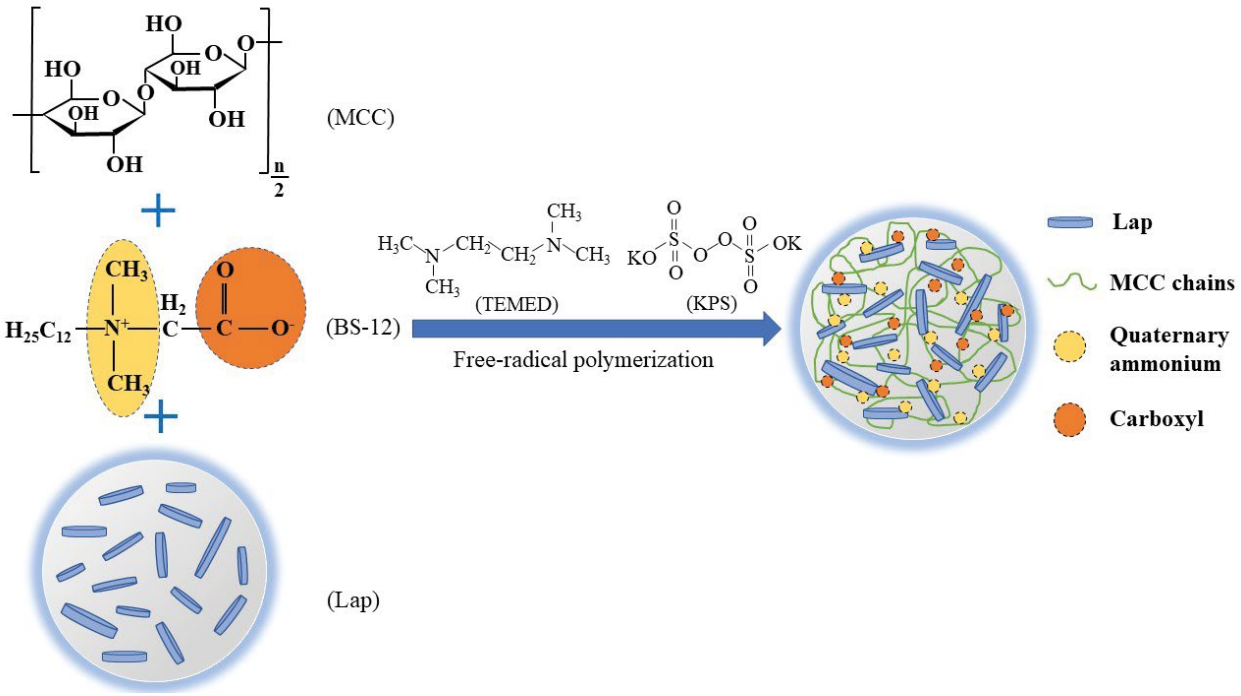

Fig. 1. Schematic illustration for synthesis of AC/Lap-Hy.

an FTIR (Nicolet iS10, USA) using the KBr pellet technique. Crystal structures of the hydrogels were determined by an X-ray diffractometer (XRD, Bruker D8, Germany) with the diffraction angle from 10° to 80°. To investigate the pyrolysis behavior of the samples, thermogravimetric analysis (TGA) curves were recorded by using a thermogravimetric analyzer (TGA, Perkin Elmer STA8000, USA) in a nitrogen atmosphere.

2.4. Swelling property experiment

0.1 g of dry hydrogel was immersed into 500 mL of deionized water, after a certain time, the hydrogel was taken out and wiped off its surface moisture, and then weighed. The swelling ratio (SR_t, g/g) was computed by Eq. (1):

$$SR_t = \frac{\left(W_t - W_d\right)}{W_d} \tag{1}$$

where W_d and W_t (g) are the mass of dry hydrogel and swollen hydrogel at time t, respectively.

2.5. Adsorption experiments

Adsorption tests in the single phosphate or ammonium system were performed by adding the hydrogels (0.1 g) into 50 mL solutions containing different concentrations of phosphate or ammonium in 150 mL flasks. Then the flasks were shaken at 150 rpm to finish the adsorption reaction. After adsorption, the hydrogels and residual solutions were separated by 0.45 μm of microfiltration membrane. The concentration of phosphate and ammonium were measured by molybdenum blue and Nessler reagent spectrophotometric methods, respectively, using a UV-Vis spectrophotometer (UV-2600, Shimadzu, Japan). The adsorption capacity q_e (mg/g) at equilibrium was estimated by the following equation.

$$q_e = \frac{\left(C_0 - C_e\right)V}{W} \tag{2}$$

where C_0 and C_e (mg/L) are the initial and equilibrium concentrations of pollutant solutions, respectively; V (mL) is the volume of solutions, and W (mg) is the mass of the adsorbents used.

The influence of pH on adsorption capacity was studied within the pH ranged from 2.0 to 12.0 with the phosphate or ammonium concentration of 50 mg/L and the contact time of 24 h at 298 K. Adsorption kinetics were carried out at 50 mg/L of phosphate or ammonium solutions at 298 K, pH 6.0 and the residual concentration was determined at predetermined time intervals from 15 to 1,440 min. Adsorption isotherms were performed at 298 K and pH 6.0 with the concentrations of phosphate or ammonium ranged from 5 to 150 mg/L under three different temperatures (288, 298, and 308 K). The effect of coexisting ions (SO_4^{2-}, CO_3^{2-}, Cl^-, NO_3^-, K^+, Na^+, Ca^{2+}, and Mg^{2+}) with concentrations range of 0.001–0.1 mol/L were conducted at 50 mg/L of phosphate or ammonium solution at 298 K and pH 6.0. The desired concentrations of salt solution were prepared by adding 0.05, 0.5, and 5 mmol of salt reagents (sulfate, carbonate, chloride, nitrate, potassium salts, sodium salt, calcium salt, and magnesium salt) into 50 mg/L of phosphate

or ammonium solutions, respectively. For co-adsorption of phosphate and ammonium in binary system, the mixture solutions (50 mL) were prepared by varying phosphate or ammonium concentration (ranged from 5 to 150 mg/L) with another one fixed (50 mg/L).

2.6. Desorption and reuse experiment

Regeneration of AC/Lap-Hy was examined by using 0.1 mol/L of NaOH and HCl solutions. 0.1 g of AC/Lap-Hy adsorbent was immersed into 50 mL of the binary solution (contained 50 mg/L of phosphate and ammonium, respectively). After accomplishment of the adsorption, AC/Lap-Hy with both phosphate and ammonium adsorbed was successively added into 40 mL of NaOH and HCl solution, respectively, regenerating for 1 h. The hydrogels were then withdrawn and determined the concentrations of phosphate and ammonium in the solution. After the desorption, the regenerated AC/Lap-Hy was separated and washed with deionized water, then dried at 373 K for next adsorption–desorption cycle using. The experiments were carried out for five cycles, and the desorption efficiency can be estimated by Eq. (3) [25]:

$$\text{Desorption efficiency}(\%) = \frac{\text{Desorbed concentration}(\text{mg/L})}{\text{Adsorbed concentration}(\text{mg/L})} \times 100\% \quad (3)$$

2.7. Practical application in real water

Two kinds of water samples including domestic sewage and river water were used to investigate the practical application of AC/Lap-Hy. 0.1 g of AC/Lap-Hy was added into different water samples for adsorption test at 150 rpm under 298 K for 24 h. Then, the residual phosphate and ammonium were determined. Domestic sewage and river water acquired from Quyang sewage treatment plant (Shanghai, China) and the tributary of Huangpu River behind University of Shanghai for Science and Technology (Shanghai, China), respectively.

3. Results and discussion

3.1. Characterizations

The SEM images of AC/Lap-Hy, C/Lap-Hy, and C-Hy are shown in Fig. 2. It is observed that C-Hy (Fig. 2a) exhibits a 3D architecture with interconnected pores of 50–100 μm in size. With introducing of Lap (C/Lap-Hy, Fig. 2b), coarse surfaces appear and the clays are found slightly aggregated in the hydrogel matrix, which might be due to the strong hydrogen bonding and ionic interaction between Lap and polymer. The AC/Lap-Hy (Fig. 2c) shows significant change in the interconnected pore morphology after modified with BS-12, which shows smaller size of 10–30 μm and thinner pore wall. Such structure is benefit for improving its adsorption property owning to the increase of water absorbability and diffusivity of adsorbate into hydrogels [26]. Furthermore, under the high magnification of 2000× (Fig. 2d), it can be observed that the Lap disperses uniformly throughout the AC/Lap-Hy, which might account for the successful intercalation of zwitterionic surfactant into Lap.

The specific surface areas and pore volumes of AC/Lap-Hy, C/Lap-Hy, and C-Hy are presented in Table 1. C/Lap-Hy shows a larger specific surface area and pore volume (13.19 m^2/g and 0.009 cm^3/g, respectively) than that of C-Hy (3.98 m^2/g and 0.003 cm^3/g, respectively), which might be attributed to the incorporation of Lap. After modified with BS-12 surfactant, the BET surface area and pore volume of AC/Lap-Hy (7.16 m^2/g and 0.004 cm^3/g, respectively) decrease since the interlayer space of Lap are blocked by loaded surfactant. Similar results were reported in previous researches [20,27].

FTIR spectra of the three hydrogels are shown in Fig. 3. Some characteristic adsorption peaks of all samples, including stretching vibration of –OH at the width band between 3,100 and 3,500 cm^{-1} [3,28], asymmetric stretching vibration of $–CH_2–$ at 2,910 cm^{-1} [29], stretching vibration of –COOR at 1,400 and 1,550 cm^{-1} [17] and stretching vibration of C–O at 1,100 cm^{-1} [30] are observed and demonstrate a successful preparation of cellulose hydrogels. After incorporating with Lap, the spectra of C/Lap-Hy and AC/Lap-Hy show additional new peak at 998 cm^{-1} attributing to the stretching vibration of Si–O [31]. Besides, the bands between 3,100 and 3,500 cm^{-1} become weaker, indicating the occurrence of the cross-linking reaction between Lap and polymer. As for AC/Lap-Hy, the peak at 1,620 cm^{-1} corresponds to stretching vibration of C=O, indicating the graft of carboxyl groups onto the molecular chain of cellulose hydrogel [32]. The peak at 1,590 cm^{-1} is designated as the stretching vibration of N–H on the quaternary ammonium group [33]. These results confirm that BS-12 with the required functional groups (carboxyl and quaternary ammonium groups) are successfully grafted onto cellulose hydrogel.

Fig. 4 shows the XRD patterns of the as-prepared samples. It can be seen from Fig. 4 that C-Hy shows typical cellulose II crystal structure at characteristic peaks of $2\theta = 20.12°$ and 22.20° [34]. After the incorporation of Lap, most characteristic peaks of Lap ($2\theta = 20.5°$, 26.2°, 34.8°, 53.4°, and 60.8°) couldn't be observed, indicating the destruction of pristine Lap crystalline structure by cross-linking process during the preparation of C/Lap-Hy [30]. Furthermore, the crystalline peaks in the AC/Lap-Hy diffractogram increase significantly, which might be attributed to the graft of BS-12 onto cellulose hydrogel molecular chain [35]. This can prove that the modification of BS-12 is conducive to the formation of good crystalline structure of AC/Lap-Hy.

TGA thermograms of AC/Lap-Hy, C/Lap-Hy, and C-Hy are shown in Fig. 5. The TGA curve of C-Hy displays three-stage mass loss: the mass loss below 220°C is due to the removal of water molecules in the interlayer and on the surface of the hydrogel, while that at 220°C–500°C attributing to the pyrolysis of polymer [36], and the third mass loss above 500°C corresponding to further decomposition of C-Hy [37]. According to the TGA result of C/Lap-Hy, especially at the temperature range from 220°C to 500°C, the mass loss of cellulose hydrogel shows slightly decrease with the addition of Lap. This improved thermal stability might be attributed to the enhancement of hydrogel network cross-link density by adding of Lap cross-linker

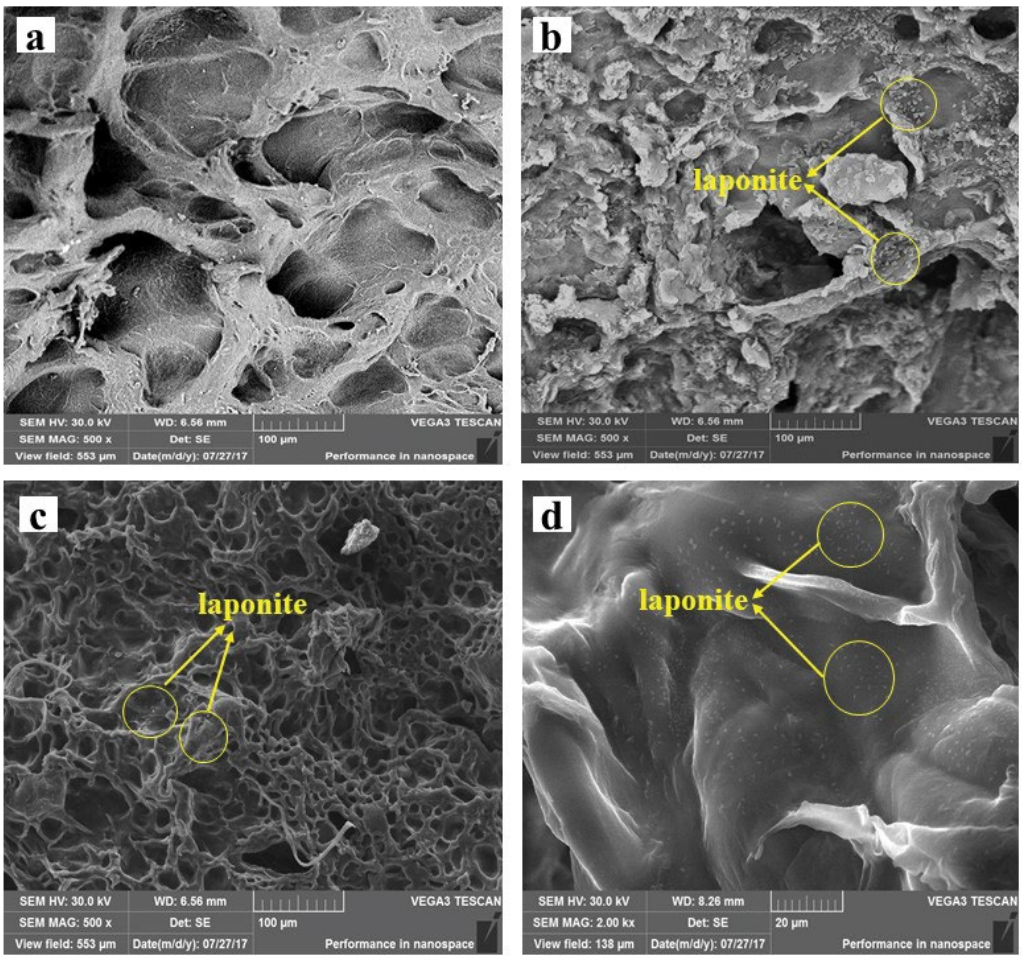

Fig. 2. SEM images of (a) C-Hy (×500), (b) C/Lap-Hy (×500), (c) AC/Lap-Hy (×500), and (d) AC/Lap-Hy (×2000).

Table 1
Specific surface area, pore characteristic, and average particle size of C-Hy, C/Lap-Hy, and AC/Lap-Hy

Adsorbent	BET (S_{BET}, m^2/g)[a]	Pore volume (V_{pore}, cm^3/g)[b]	Average pore size (D_p, nm)[c]
C-Hy	3.98	0.003	30.47
C/Lap-Hy	13.19	0.009	22.09
AC/Lap-Hy	7.16	0.004	3.06

[a]BET specific surface.
[b]Total pore volume measured at $p/p_0 = 0.99$.
[c]Average pore diameter calculated from the desorption branch of the isotherm using the BJH method.

[29]. As for AC/Lap-Hy, the shift of mass loss peak for first stage to higher temperature of 250°C might be due to the interfacial reaction between hydrogel and BS-12 surfactant [38], and the increase of mass loss at second stage is due to the further decomposition of intercalated surfactant [39]. When temperature increases to 700°C, the residual mass percent of C-Hy, C/Lap-Hy, and AC/Lap-Hy decrease to 33%, 37%, and 25%, respectively. Although AC/Lap-Hy presents lower thermal stability than Lap-Hy and C-Hy between 100°C and 700°C, it still exhibits good stability under ambient temperature (<100°C).

3.2. Swelling property

The capacity of swelling is one of the most important parameters to evaluate the property of hydrogels [29]. The swelling behaviors in distilled water at 298 K are depicted in Fig. 6. Characteristics of swelling kinetics curves indicate a fast swelling ratio at the first 2 h, and the swelling equilibrium reaches at about 6 h. Compared with C-Hy, introducing Lap into the hydrogel network decreases its swelling ratio, owing to the fact that the interaction between Lap and hydrogel molecular chain will increase the number of crosslink points and lead to the decrease of its swelling ratio. Shen et al. [29] and Mahdavinia et al. [40] also reported the similar results. Furthermore, AC/Lap-Hy exhibits higher swelling capacity than both C-Hy and C/Lap-Hy, this might be ascribed to the increase of carboxylate and quaternary ammonium groups on the hydrogel molecular chains, which results in a higher mobile ions concentration inside the hydrogel rather than the surrounding medium and finally leads to the swelling of hydrogel [41]. Besides, the higher porosity and thinner walls of AC/Lap-Hy in SEM observation could promote the transportation of

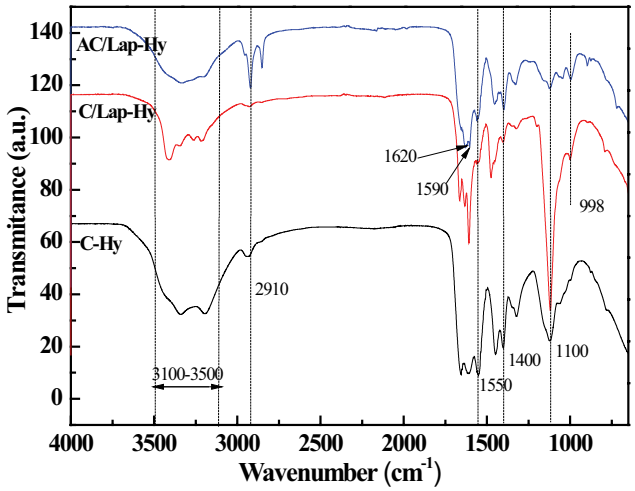

Fig. 3. FTIR spectra of C-Hy, C/Lap-Hy, and AC/Lap-Hy.

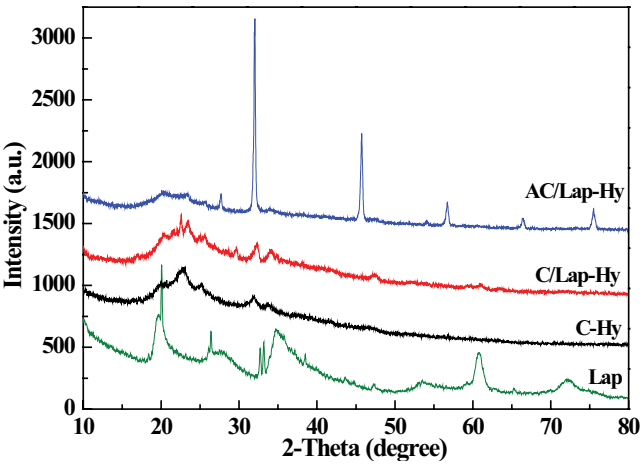

Fig. 4. XRD patterns of pristine Lap, C-Hy, C/Lap-Hy, and AC/Lap-Hy.

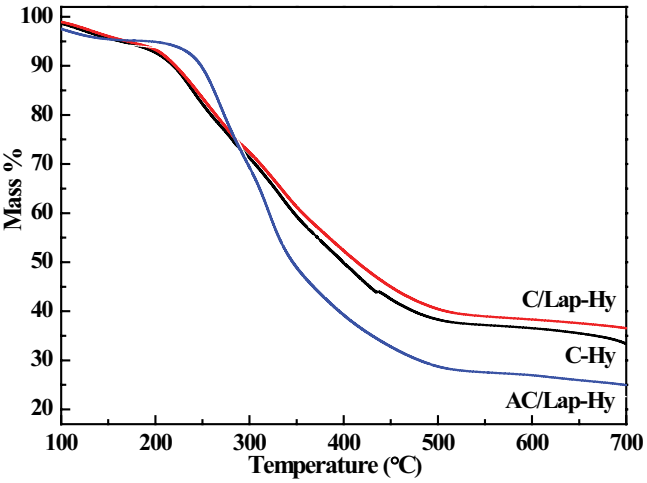

Fig. 5. TGA curves of C-Hy, C/Lap-Hy, and AC/Lap-Hy.

water molecules and shorten the distance across the porous structure, thus facilitating the relaxation of polymer chains.

Eq. (4) is often used to describe the swelling processes of hydrogels, and eventually to reveal the mechanisms of water diffusion in hydrogel matrices [42]:

$$F = \frac{(W_t - W_d)}{(W_e - W_d)} = Kt^n \quad (4)$$

where W_d (g) is the mass of dry hydrogel, W_t (g) is the mass of swollen hydrogel at time t, W_e (g) is the mass of swollen hydrogel at equilibrium time, K (g/g s) is the swelling constant related to hydrogel structure, and n is swelling exponent. The value of n indicating of non-Fickian diffusion between 0.5 and 1, and for Fickian diffusion when ≤0.5 [43]. The value of n for all samples in this study are above 0.5, illustrating a non-Fickian diffusion transport mode of water into the hydrogel (Table 2).

3.3. Adsorption study

3.3.1. Influence of initial solution pH

The influences of pH on the removal efficiency of ammonium and are presented in Fig. 7. Generally, the phosphate removal efficiencies of C-Hy, C/Lap-Hy, and AC/Lap-Hy increase with pH rising to 6.0 and decrease steadily as pH further increases to 12.0 (Fig. 7a). The dissociation

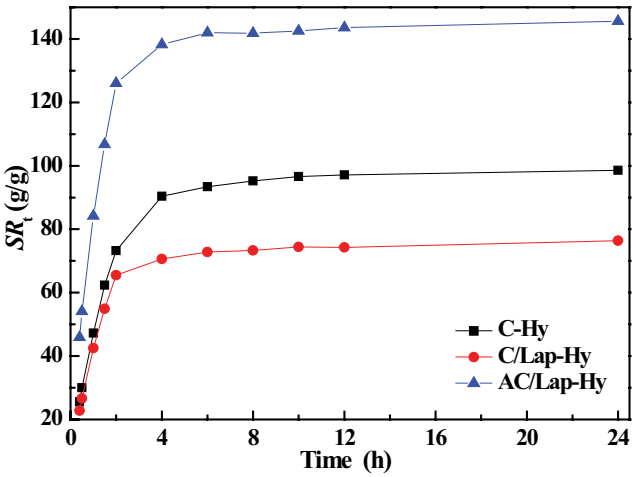

Fig. 6. Swelling kinetics of C-Hy, C/Lap-Hy, and AC/Lap-Hy.

Table 2
Swelling kinetics parameters for C-Hy, C/Lap-Hy, and AC/Lap-Hy

Adsorbent	S_{pra} (g/g)	Swelling kinetics parameters		
		n	K (g/g s)	R^2
C-Hy	98.6	0.659	3.21×10^{-2}	0.9994
C/Lap-Hy	76.4	0.657	3.72×10^{-2}	0.9996
AC/Lap-Hy	145.6	0.625	4.38×10^{-2}	0.9990

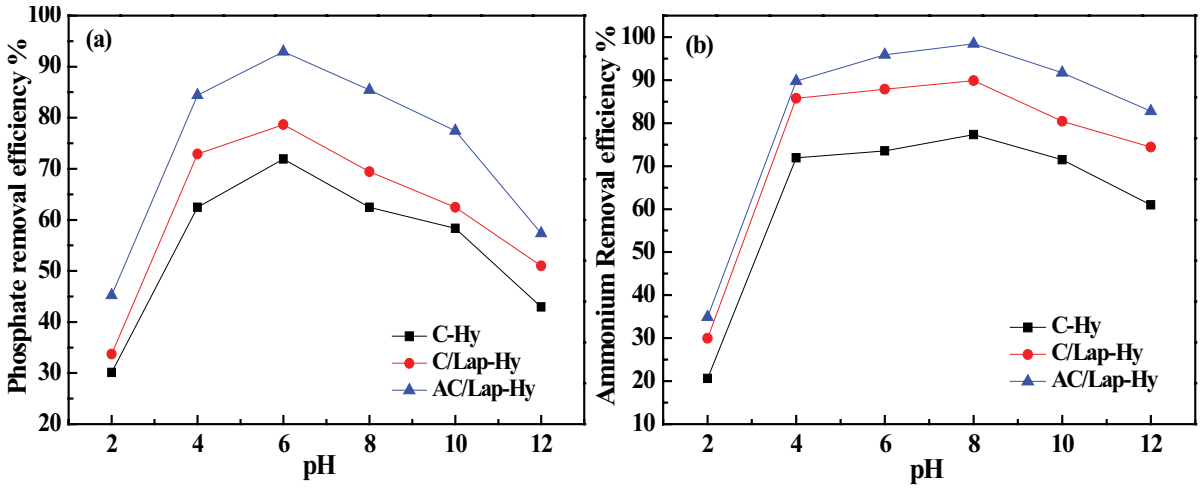

Fig. 7. Effect of pH values on the removal efficiency of (a) phosphate and (b) ammonium onto C-Hy, C/Lap-Hy, and AC/Lap-Hy.

equilibrium of phosphate is largely determined by pH value [44]. When pH < 2.16, H_3PO_4 is the major specie which cannot be adsorbed by the hydrogels, resulting to a poor removal rate [45]. As pH increases to 7.20, the ratio of H_3PO_4 decreases and that of $H_2PO_4^-$ rapidly peaks, leading to the generation of surface complexes between $H_2PO_4^-$ and –OH group on the adsorbent surfaces. Besides, the protonation of hydroxyl groups in the acidic region could enhance the electrostatic attraction between them, which facilitates phosphate adsorption [46]. At alkaline pH, OH^- ions will compete with the adsorption of phosphate anion, since they can change the surface charge of hydrogel by occupying adsorption sites [47]. The ammonium adsorption behavior exhibits a significantly rise when pH increases from 2.0 to 4.0, then it maintains stable at pH 4.0–8.0 (Fig. 7b). Furthermore, the removal efficiency of ammonium decreases when pH increases to above 8.0. At lower pH (pH < 4.0), partial –COO^- is protonated, leading to the diminishment of electrostatic attraction between ammonium and hydrogel, and thus results to a low adsorption capacity of ammonium [48]. At higher pH (pH > 8.0), ammonium is neutralized by hydroxyl ion and the ion strength of ammonium is also increased, leading to the decrease of its removal efficiency. From the experimental results obtained above, the optimal pH value for phosphate and ammonium adsorption is at 6.0 and 8.0, respectively.

For comparison, C-Hy exhibits the lowest removal efficiency of phosphate (71.9%) and ammonium (77.3%) at optimal pH value. After the incorporation of Lap (C/Lap-Hy), the removal efficiency of ammonium increases to 89.9% while the removal efficiency of phosphate only rises slightly (78.7%). This might be due to that the negatively charged Si–O^- and positively charged Na^+ in the layers of Lap could provide the bind site onto C/Lap-Hy according to electrostatic attraction and cationic exchange, and improve its adsorption for ammonium [49]. Besides, the higher specific surface area and pore volume of C/Lap-Hy also contributes to a higher adsorption property. When modified with BS-12 (AC/Lap-Hy), the removal efficiency of phosphate and ammonium both enhance significantly (93.0% for phosphate and 98.5% for ammonium), indicating that AC/Lap-Hy with both positively (quaternary ammonium) and negatively (carboxyl) charged groups could strongly attract the opposite charged ions based on electrostatic attraction, which will retain its zwitterionic characteristic over a broad pH range. Although AC/Lap-Hy has lower specific surface area and pore volume, it also has higher adsorption capacity rather than C/Lap-Hy. As a result, the functional groups on the surface of adsorbent have strong interaction with the pollutants, which contributes to its adsorption performance largely, indicating that chemisorption might be the predominant mechanism during the adsorption process [50].

3.3.2. *Adsorption kinetics*

The effects of contact time on the adsorption capacity of phosphate and ammonium are shown in Fig. 8. The obtained results show a rapid adsorption at initial hours, which is due to the abundant available adsorption sites at initial adsorption phase [39]. As the adsorption goes on, the adsorption becomes slower until the equilibrium reaches, indicating the decrease of the adsorption rate of phosphate and ammonium, which results in the saturation adsorption in the final step. The adsorption equilibrium of phosphate in all samples is approximately 360 min, whereas the adsorption equilibrium of ammonium is approximately 480 min.

Moreover, pseudo-first-order [Eq. (5)], pseudo-second-order [Eq. (6)], and Elovich [Eq. (7)] kinetic models are used to investigate the adsorption process and determine the most appropriate one [51–53].

$$\log\left(q_e - q_t\right) = \log q_e - \frac{k_1 t}{2.303} \tag{5}$$

$$\frac{t}{q_t} = \frac{1}{k_2 q_e^2} + \frac{t}{q_e} \tag{6}$$

$$q_t = \frac{1}{\beta}\ln\alpha\beta + \frac{1}{\beta}\ln t \tag{7}$$

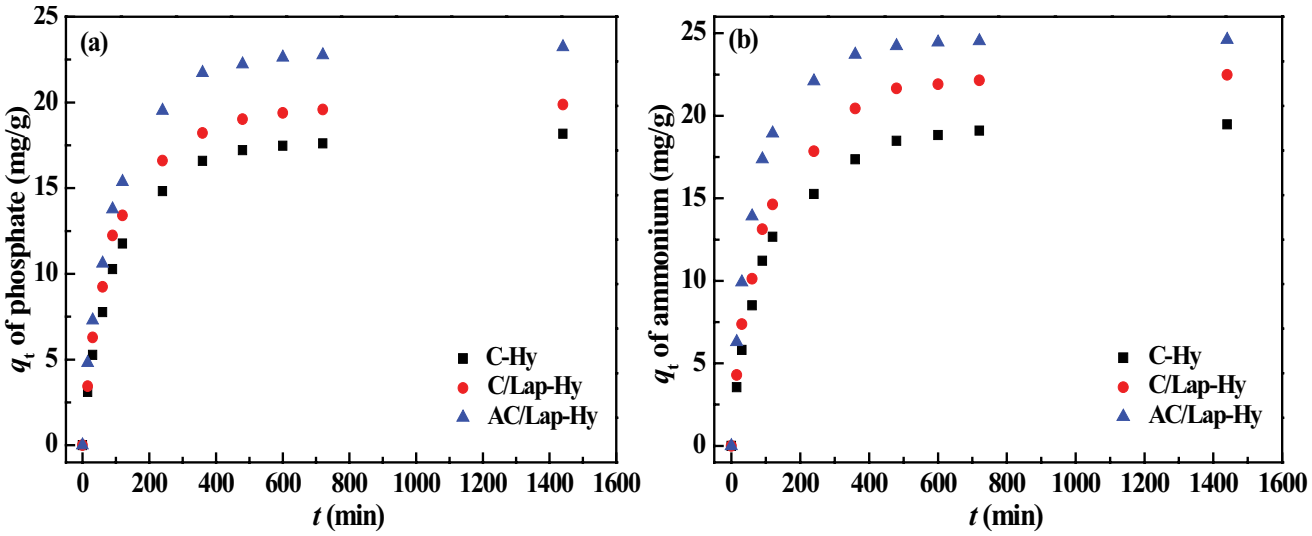

Fig. 8. Adsorption kinetics of (a) phosphate and (b) ammonium onto C-Hy, C/Lap-Hy, and AC/Lap-Hy.

where q_t (mg/g) and q_e (mg/g) are the amount of pollutants adsorbed at time t and at equilibrium time, respectively; k_1 (1/min) and k_2 (g/mg min) are the rate constants of the pseudo-first-order and pseudo-second-order kinetic models, respectively. The product h represents the initial adsorption rate ($h = k_2 q_e^2$). In addition, α (mg/g) is the initial adsorption rate constant, and β (g/mg) is the desorption rate constant. The three kinetic equations [Eqs. (5)–(7)] provide a good fit according to the correlation coefficients (R^2) values and are applicable in the following order: pseudo-second-order > Elovich > pseudo-first-order (Table 3). Also, the adsorption capacity of $q_{e,\exp}$ and $q_{e,\text{cal}}$ (calculated from pseudo-second-order model) are almost coincident. It could be concluded that the pseudo-first-order kinetic model is the most suitable for describing the phosphate and ammonium adsorption. This phenomenon illustrates that the adsorption of phosphate and ammonium by hydrogels is related to the chemisorption mechanism [21].

3.3.3. Adsorption isotherms

The influences of initial concentration of phosphate and ammonium on their adsorption capacity using C-Hy, C/Lap-Hy, and AC/Lap-Hy at different temperatures (288, 298, and 308 K) are presented in Fig. 9. The equilibrium adsorption capacity rapidly increases with the increasing concentration of phosphate and ammonium firstly, and then tends to equilibrium until the available adsorption sites are saturated. Furthermore, the adsorption capacity of ammonium decreases with increasing of temperature while increases for the adsorption capacity of phosphate, indicating the exothermic and endothermic process for phosphate and ammonium adsorption, respectively.

Table 3
Pseudo-first-order, pseudo-second-order, and Elovich kinetic parameters of phosphate and ammonium onto C-Hy, C/Lap-Hy, and AC/Lap-Hy

Kinetic models	Parameter	Phosphate			Ammonium		
		C-Hy	C/Lap-Hy	AC/Lap-Hy	C-Hy	C/Lap-Hy	AC/Lap-Hy
Pseudo-first-order	$q_{e,\exp}$ (mg/g)	18.2	19.9	23.2	19.5	22.5	24.6
	q_e (mg/g)	13.8	16.3	18.9	15.7	16.5	17.8
	k_1 (1/min)	5.53×10^{-3}	6.68×10^{-3}	7.14×10^{-3}	5.53×10^{-3}	5.58×10^{-3}	6.91×10^{-3}
	R^2	0.9778	0.9960	0.9958	0.9933	0.9886	0.9794
Pseudo-second-order	q_e (mg/g)	19.3	21.0	24.5	20.7	23.8	25.6
	k_2 (g/mg/min)	7.01×10^{-4}	7.36×10^{-4}	6.46×10^{-4}	6.58×10^{-4}	6.20×10^{-4}	9.94×10^{-4}
	H (mg/g/min)	0.261	0.325	0.388	0.282	0.351	0.650
	R^2	0.9994	0.9993	0.9992	0.9993	0.9991	0.9994
Elovich	α (mg/g)	0.522	0.636	5.390	0.591	0.725	1.243
	β (g/mg)	0.232	0.214	0.185	0.225	0.195	0.185
	R^2	0.9931	0.9947	0.9916	0.9948	0.9961	0.9863

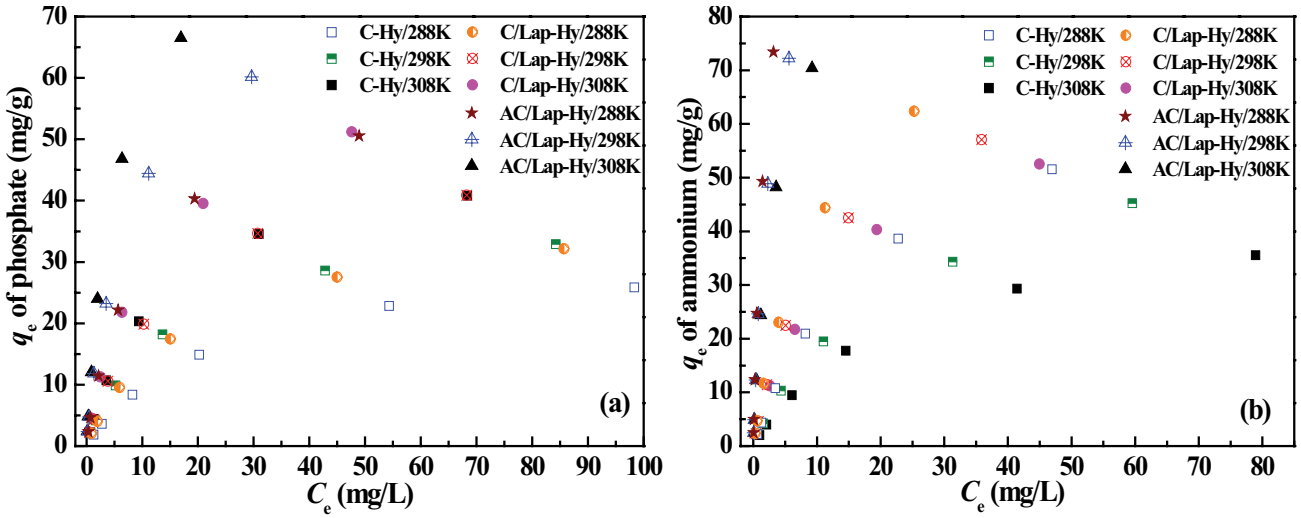

Fig. 9. Adsorption isotherms of (a) phosphate and (b) ammonium onto C-Hy, C/Lap-Hy, and AC/Lap-Hy.

Langmuir and Freundlich model are used to describe the adsorption isotherms. The relevant isotherm equations are shown as below [54]:

$$q_e = \frac{q_m K_L C_e}{1 + K_L C_e} \tag{8}$$

$$q_e = K_F C_e^{1/n} \tag{9}$$

where C_e (mg/L) is the equilibrium pollutants concentration, q_e (mg/g) is the adsorption capacity at equilibrium, q_m (mg/g) is the maximum adsorption capacity of pollutants, K_L (L/mg) is the Langmuir coefficient related to the affinity of the binding site, K_F (mg/g) and n are the Freundlich constants.

At all three temperature, the adsorption of phosphate and ammonium can be well described by Langmuir model rather than Freundlich model (Table 4). Moreover, the maximum adsorption capacity calculated from Langmuir

Table 4
Langmuir and Freundlich isotherm parameters for adsorption of phosphate and ammonium onto C-Hy, C/Lap-Hy, and AC/Lap-Hy at different temperatures

Pollutant	Adsorbent	Temperature (K)	Langmuir model			Freundlich model		
			q_m (mg/g)	K_L (L/mg)	R^2	K_F (mg/g)	n	R^2
Phosphate	C-Hy	288	31.7	4.57×10^{-2}	0.9995	1.90	1.62	0.9716
		298	38.2	7.12×10^{-2}	0.9992	3.10	1.71	0.9678
		308	48.3	8.05×10^{-2}	0.9999	3.93	1.62	0.9642
	C/Lap-Hy	288	38.5	5.79×10^{-2}	0.9993	2.66	1.64	0.9705
		298	49.0	7.22×10^{-2}	0.9993	3.70	1.60	0.9709
		308	63.3	8.51×10^{-2}	0.9992	5.01	1.50	0.9720
	AC/Lap-Hy	288	59.5	1.12×10^{-1}	0.9994	5.76	1.59	0.9668
		298	74.6	1.38×10^{-1}	0.9990	8.00	1.49	0.9748
		308	87.7	1.83×10^{-1}	0.9996	11.31	1.39	0.9749
Ammonium	C-Hy	288	73.5	4.95×10^{-2}	0.9996	3.71	1.36	0.9842
		298	56.5	5.06×10^{-2}	0.9992	3.13	1.46	0.9786
		308	45.3	4.51×10^{-2}	0.9994	2.43	1.51	0.9771
	C/Lap-Hy	288	89.3	8.95×10^{-2}	0.9993	6.86	1.34	0.9835
		298	76.9	8.08×10^{-2}	0.9999	5.56	1.39	0.9766
		308	67.6	7.63×10^{-2}	0.9995	4.85	1.45	0.9772
	AC/Lap-Hy	288	123.5	4.60×10^{-1}	0.9994	34.72	1.24	0.9890
		298	105.3	3.88×10^{-1}	0.9996	24.32	1.31	0.9838
		308	96.2	2.90×10^{-1}	0.9996	17.43	1.36	0.9812

model is closer to the experimental data. AC/Lap-Hy obtains the highest maximum adsorption capacities of 74.6 mg/g for ammonium and 105.3 mg/g for phosphate rather than C/Lap-Hy and C-Hy at the temperatures of 298 K, which is consistent with the results of swelling capacity presented in Fig. 6. This might be due to the fact that swelling behavior of hydrogel is an important factor in its adsorption ability. Higher swelling ratio indicates a larger pore size inside the hydrogel network, which facilitates the diffusion of ions into hydrogel and the coordination of ions with the functional groups on hydrogel [8]. Besides, the higher adsorption capacity of ammonium indicates stronger interaction between binding sites and ammonium rather than phosphate. As a result, the monolayer adsorption of phosphate and ammonium occurs on the hydrogels.

Although some other bio-adsorbents have been used to remove phosphate or ammonium from water (Table 5), bio-hydrogel that could simultaneously adsorb phosphate and ammonium are seldom reported. And AC/Lap-Hy also shows comparable adsorption capacity and speed as an amphoteric adsorbent, which indicates that it is an excellent candidate absorbent for application to eutrophication water treatment.

3.3.4. Adsorption thermodynamics

Thermodynamic parameters are determined to evaluate the spontaneous nature and thermodynamic behavior of the adsorption process. The variations including Gibbs free energy ($\Delta G°$, kJ/mol), enthalpy ($\Delta H°$, kJ/mol), and entropy ($\Delta S°$, J/mol K) are calculated by Eqs. (10) and (11) [39]:

$$\ln K_d = \frac{\Delta S°}{R} - \frac{\Delta H°}{RT} \tag{10}$$

$$\Delta G° = \Delta H° - T\Delta S° \tag{11}$$

where R (8.314 J/mol K) is gas constant, T (K) is Kelvin temperature, and K_d (L/g) is adsorption equilibrium constant of Langmuir isotherm [54]. The values of $\Delta H°$ and $\Delta S°$ are obtained from the slope and intercept of the linear plot of $\ln K_d$ vs. $1/T$, and the corresponding parameters are presented in Table 6. The negative values of $\Delta G°$ at all temperatures reveal the spontaneous and feasible adsorption process for phosphate and ammonium onto the hydrogels. In additionally, the positive value of $\Delta H°$ for phosphate adsorption depicts the endothermic behavior, implying the higher adsorption capacity of phosphate at higher temperature, whereas the negative value for ammonium adsorption shows an exothermic nature. The value of $\Delta S°$ for the phosphate adsorption reaction are found to be positive, illustrating the increasing randomness at the solid–liquid interfaces, while the negative $\Delta S°$ reflects orderly adsorbed of ammonium on the surface of hydrogels.

3.3.5. Influence of coexisting ions

Effects of the coexisting anions and cations species (SO_4^{2-}, CO_3^{2-}, Cl^-, NO_3^-, K^+, Na^+, Ca^{2+}, and Mg^{2+}) on adsorption capacity of phosphate and ammonium onto AC/Lap-Hy are examined, and the results are displayed in Fig. 10. It can be seen from Fig. 10a that the adsorption capacities of phosphate decrease from 23.24 to 19.70, 18.23, 21.44, and 22.02 mg/L, respectively as the concentrations of SO_4^{2-}, CO_3^{2-}, Cl^-, and NO_3^- increase from 0 to 0.1 mol/L. It is possible that coexisting anions in the solution will have competitive adsorption with phosphate toward hydrogel, indicating the generation of outer-sphere surface complexes during the adsorption [32]. Moreover, the adsorption of multivalent anions is stronger than monovalent anions [53], as a result, the hindrance effect of CO_3^{2-} and SO_4^{2-} for phosphate adsorption are bigger than that of Cl^- and NO_3^-. While the presence of cations will promote the adsorption of phosphate. The K^+, Ca^{2+}, and Mg^{2+} might react with phosphate to form potassium phosphate, calcium phosphate, and magnesium phosphate, respectively [60]. Fig. 10b shows that

Table 5
Comparison of the maximum adsorption capacities of phosphate and ammonium onto various adsorbents

Adsorbents	Temperature (K)	q_m (mg/g)		References
		Phosphate	Ammonium	
Fe(III)-doped chitosan	303	15.7	/	[44]
$La(OH)_3$ loaded magnetic cationic hydrogel	298	90.2	/	[47]
Polyvinyl alcohol hydrogel	303	11.5	/	[55]
Mg-Al-modified biochar	298	74.5	/	[7]
Fe_2O_3 loaded graphite-like carbon nitride	297	52.5	/	[56]
La-modified layered chalcogenide	298	24.4	/	[57]
Starch-based nanocomposite hydrogel	298	/	7.4	[1]
Polyvinyl alcohol/acrylic acid/tourmaline hydrogel	303	/	42.7	[48]
Chitosan grafted poly(acrylic acid)/unexpanded vermiculite	303	/	78.2	[10]
MgO impregnated biochar: sugarcane leaf trash		/	22.0	[58]
Modified clinoptilolite	303	2.0	2.0	[59]
MgO-coated natural diatomite	298	160.94	77.05	[60]
AC/Lap-Hy	298	74.6	105.3	Present study

Table 6
Values of thermodynamic parameters for adsorption of phosphate and ammonium onto the C-Hy, C/Lap-Hy, and AC/Lap-Hy

Pollutant	Adsorbent	Temperature (K)	$\Delta G°$ (kJ/mol)	$\Delta H°$ (kJ/mol)	$\Delta S°$ (J/mol K)
Phosphate	C-Hy	288	–0.976	36.552	130.305
		298	–2.279		
		308	–3.582		
	C/Lap-Hy	288	–1.924	32.565	119.755
		298	–3.122		
		308	–4.319		
	AC/Lap-Hy	288	–4.518	32.498	128.526
		298	–5.803		
		308	–7.088		
Ammonium	C-Hy	288	–3.139	–21.277	–62.981
		298	–2.509		
		308	–1.879		
	C/Lap-Hy	288	–4.956	–16.188	–39.002
		298	–4.566		
		308	–4.176		
	AC/Lap-Hy	288	–9.703	–26.255	–57.473
		298	–9.128		
		308	–8.553		

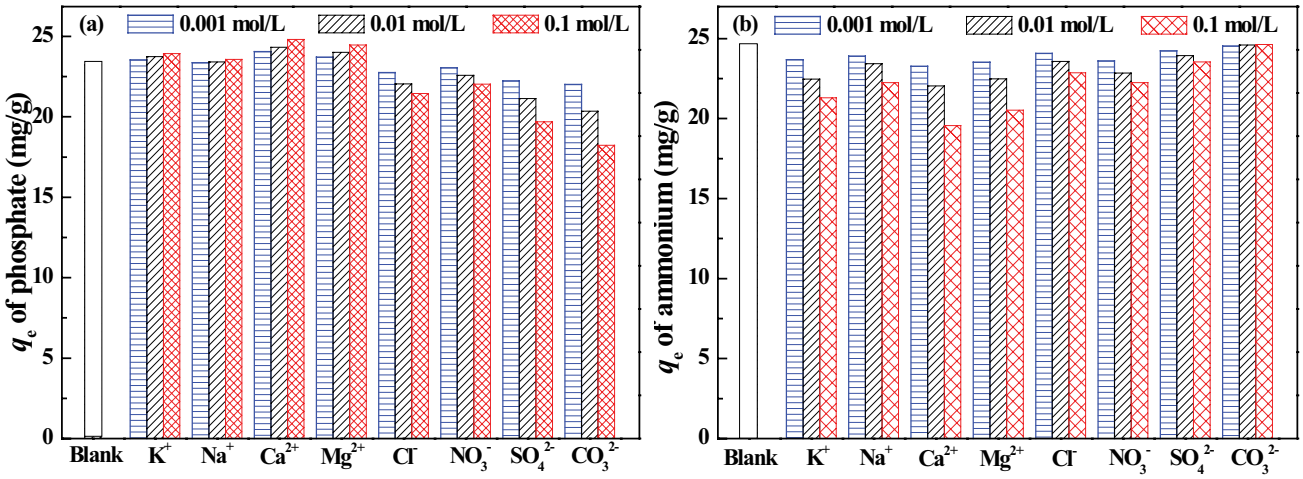

Fig. 10. Effect of coexisting cations and anions on the adsorption capacity of (a) phosphate and (b) ammonium onto AC/Lap-Hy.

the presence of cations hinder the removal of ammonium, which could also be attributed to the complete adsorption. Anions have the same effects on the adsorption of ammonium, owning to the fact that coexisting cations could occupy the adsorption sites and increase the electrostatic repulsion between hydrogel and ammonium [44].

3.3.6. Adsorption of phosphate and ammonium in the binary system

To evaluate the effect of the coexistence of phosphate and ammonium on their mutual adsorption onto AC/Lap-Hy, the binary adsorption experiments are conducted by varying phosphate and ammonium concentrations (5–150 mg/L) with another one fixed (50 mg/L), and the results are shown in Fig. 11. It can be seen that the adsorption capacity of one type of ion (phosphate/ammonium) decreases with increasing in the concentration of the other kind of ion when both of the two ions are present in solution. The adsorption capacity of ammonium decreases from 24.6 to 20.6 mg/g (reduced by 16.3%) with phosphate concentration increases from 0 to 150 mg/L while the adsorption capacity of phosphate significantly decreases by 22.6% with the increasing concentration of ammonium, which is attributed to the competitive adsorption between phosphate and ammonium for adsorption sites on AC/Lap-Hy [61]. The stronger interference of ammonium with phosphate adsorption indicates the

better affinity for ammonium than phosphate onto AC/Lap-Hy. It could be deduced that electrostatic attraction plays a major role in adsorption process.

3.4. Reusability and real water treatment

The effects of five adsorption–desorption consecutive cycles on the adsorption and desorption efficiency of phosphate and ammonium on AC/Lap-Hy are shown in Fig. 12. Removal efficiency of phosphate and ammonium are observed to decrease from 93.0% to 87.3% and from 98.5% to 94.2%, respectively, after five recycling experiments, indicating that desorption of both phosphate and ammonium are complete and the hydrogel has excellent regeneration efficiency. This result illustrates that the quaternary ammonium and carboxyl groups on AC/Lap-Hy are stable enough. This might be due to the completely three-dimensional crosslinked structure of AC/Lap-Hy [48].

AC/Lap-Hy is further used to treat the actual water (domestic sewage and polluted river water). The water quality parameters along with the concentration of phosphate and ammonium and their removal efficiencies are presented in Table 7. The removal efficiencies toward phosphate (91.7% for domestic sewage, 88.8% for river water) and ammonium (93.6% for domestic sewage, 95.9% for river water) in real water are slightly lower than that of simulated water, which might be due to the adverse effect of the presence of coexisting ions and other natural organic

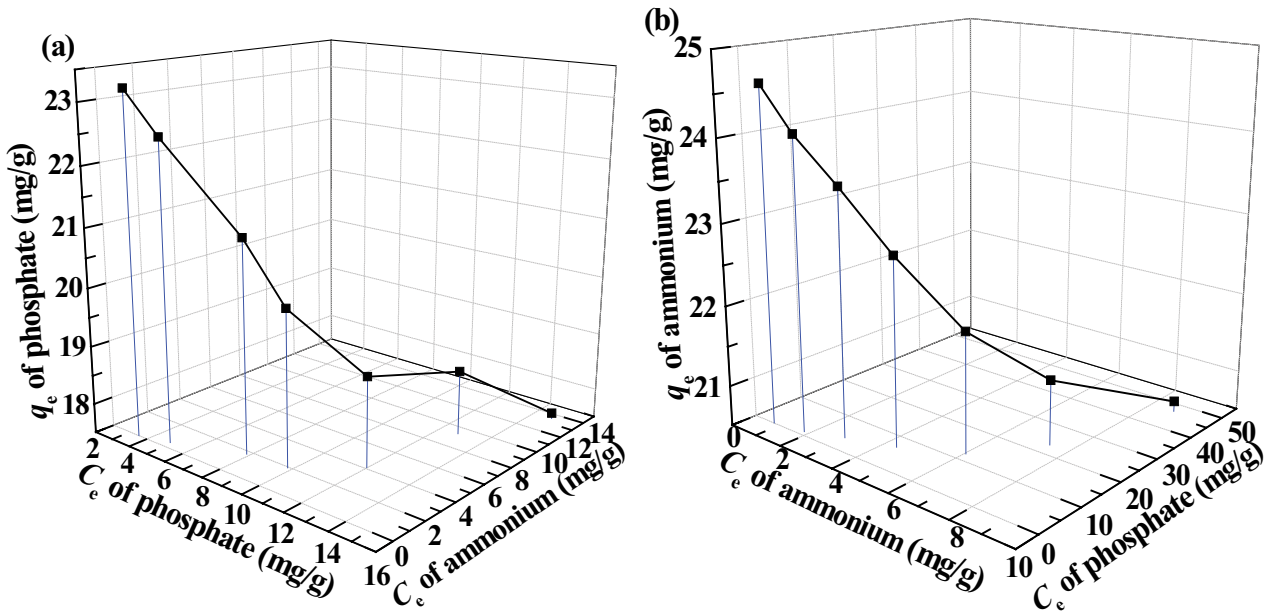

Fig. 11. Binary adsorption isotherms: the adsorption capacity of (a) phosphate and (b) ammonium was plotted against the equilibrium concentrations of phosphate and ammonium.

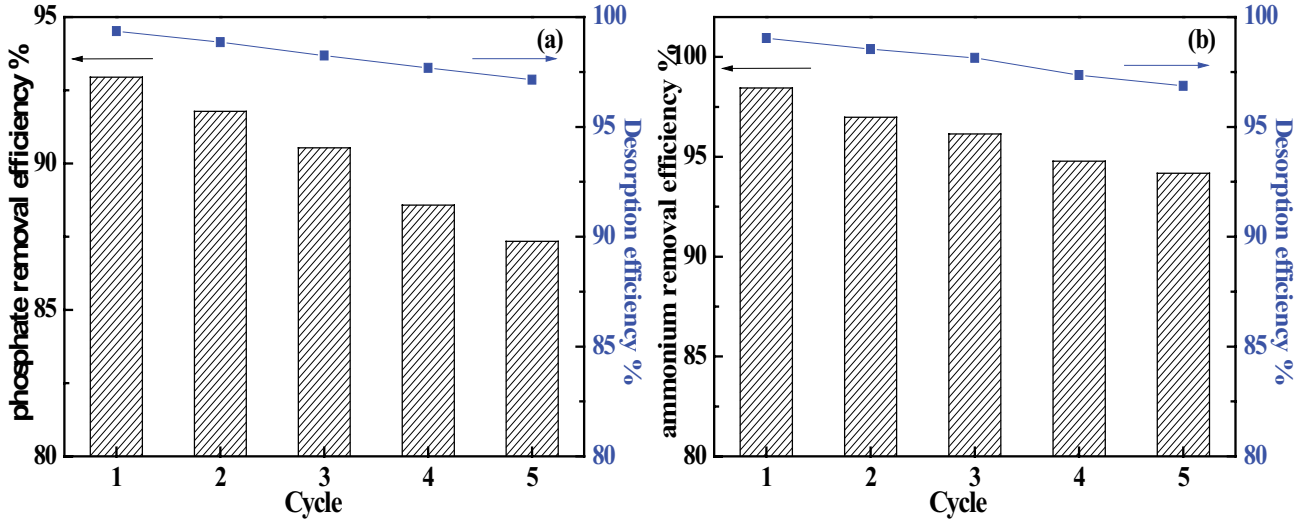

Fig. 12. Adsorption–desorption cycles of (a) phosphate and (b) ammonium onto AC/Lap-Hy.

Table 7
Adsorbent performance in phosphate and ammonium removal from water samples

Sample	Domestic sewage	River water
EC (mS/cm)	1.42	0.84
pH	7.89	6.69
$C_{Phosphate}$ (mg/L)	0.76	0.82
$C_{Ammonium}$ (mg/L)	20.97	7.51
Effluent for phosphate (mg/L)	0.063	0.092
Effluent for ammonium (mg/L)	1.34	0.31

matters [56]. However, AC/Lap-Hy still exhibits satisfactory performance in actual water and the residual concentrations of phosphate and ammonium for river water and domestic sewage effluents are below the Chinese standard of surface water environment quality and integrated wastewater discharge standard, respectively. Thus, AC/Lap-Hy is suitable for application in real water treatment.

4. Conclusion

In this work, an amphoteric cellulose/laponite nanocomposite hydrogel (AC/Lap-Hy) was synthesized for simultaneous adsorption of ammonium and phosphate from aqueous solutions. Based on the characterization results, the AC/Lap-Hy exhibited a porous structure with uniform dispersion of Lap nanoparticle, and carboxyl and quaternary ammonium groups had been successfully grafted onto the required binding sites of the cellulose hydrogel. Batch adsorption experiment results showed that AC/Lap-Hy exhibited higher maximum adsorption capacity of ammonium (105.3 mg/g) than phosphate (74.6 mg/g). The adsorption isotherm and kinetic followed Langmuir and pseudo-second-order models better, indicating monolayer chemical adsorption of phosphate and ammonium onto AC/Lap-Hy. Co-adsorption study indicated that the uptake of phosphate/ammonium was fairly reduced with the increase concentration of the other ion in solution, which revealed the antagonistic effect between phosphate and ammonium. Furthermore, the adsorption capacity of ammonium has greater impact on that of phosphate, owning to the lower affinity of the latter onto AC/Lap-Hy. All of the results demonstrated that the multiple effect of chemisorption (electrostatic attraction and/or cationic exchange) and physisorption might be responsible for the high adsorption capacity, and chemisorption might be the predominant mechanism over the adsorption process. AC/Lap-Hy was also effectively applied for the simultaneous removal of phosphate and ammonium in real wastewater such as sewage and polluted river water.

Acknowledgment

This work was sponsored financially by National Natural Science Foundation of China (No. 21806107).

References

[1] B. Shahrooie, L. Rajabi, A.A. Derakhshan, M. Keyhani, Fabrication, characterization and statistical investigation of a new starch-based hydrogel nanocomposite for ammonium adsorption, J. Taiwan Inst. Chem. Eng., 51 (2015) 201–215.
[2] Q. Zeng, L Qin, L. Bao, Y. Li, X. Li, Critical nutrient thresholds needed to control eutrophication and synergistic interactions between phosphorus and different nitrogen sources, Environ. Sci. Pollut. Res. Int., 23 (2016) 21008–21019.
[3] Y. Wang, L. Yu, R. Wang, Y. Wang, X. Zhang, Microwave catalytic activities of supported perovskite catalysts MO_x/$LaCo_{0.5}Cu_{0.5}O_3$@CM (M = Mg, Al) for salicylic acid degradation, J. Colloid Interface Sci., 564 (2020) 392–405.
[4] Y. Wang, Y. Wang, L. Yu, R. Wang, X. Zhang, Highly effective microwave-induced catalytic degradation of bisphenol A in aqueous solution using double-perovskite intercalated montmorillonite nanocomposite, Chem. Eng. J., 390 (2020) 124550.
[5] J. Chen, X. Zhang, F. Bi, X. Zhang, Y. Yang, Y. Wang, A facile synthesis for uniform tablet-like TiO_2/C derived from Materials of Institut Lavoisier-125(Ti) (MIL-125(Ti)) and their enhanced visible light-driven photodegradation of tetracycline, J. Colloid Interface Sci., 571 (2020) 275–284.
[6] L. Zhou, Y. Ga, K. Yu, H. Zhou, Y.G.D. Costa, S. Yi, W. Zhuang, Microbial community in *in-situ* waste sludge anaerobic digestion with alkalization for enhancement of nutrient recovery and energy generation, Bioresour. Technol., 295 (2020) 122277.
[7] Q.Q. Yin, R.K. Wang, Z.H. Zhao, Application of Mg-Al-modified biochar for simultaneous removal of ammonium, nitrate, and phosphate from eutrophic water, J. Cleaner Prod., 176 (2018) 230–240.
[8] Y. Wang, Y. Xiong, F.L. Sun, Y.Q. Yang, X.D. Zhang, Ultrasonic-assisted synthesis of a superabsorbent composite hydrogel for the responsive and removal properties of Pb(II), Acta Phys. Chim. Sin., 32 (2016) 753–762.
[9] Y. Wang, Y. Xiong, J.Y. Wang, X.D. Zhang, Ultrasonic-assisted fabrication of montmorillonite-lignin hybrid hydrogel: highly efficient swelling behaviors and super-sorbent for dye removal from wastewater, Colloid Surf., A, 520 (2017) 903–913.
[10] Y.A. Zheng, Y.T. Xie, A.Q. Wang, Rapid and wide pH-independent ammonium-nitrogen removal using a composite hydrogel with three-dimensional networks, Chem. Eng. J., 179 (2012) 90–98.
[11] H.T. Yeit, M.K. Li, W.M. Abdul, Synthesis of cellulose hydrogel for copper (II) ions adsorption, J. Environ. Chem. Eng., 6 (2018) 4588–4597.
[12] P.F. Luo, L.L. Liu, W.Y. Xu, L.H. Fan, M. Nie, Preparation and characterization of aminated hyaluronic acid/oxidized hydroxyethyl cellulose hydrogel, Carbohydr. Polym., 199 (2018) 170–177.
[13] H.F. Peng, X.Y. Ning, G. Wei, S.P. Wang, G.L. Dai, A.Q. Ju, The preparations of novel cellulose/phenylboronic acid composite intelligent bio-hydrogel and its glucose, pH-responsive behaviors, Carbohydr. Polym., 195 (2018) 349–355.
[14] Y. Kim, K.K. Yun, S. Kim, D. Harbottle, J.W. Lee, Nanostructured potassium copper hexacyanoferrate-cellulose hydrogel for selective and rapid cesium adsorption, Chem. Eng. J., 313 (2017) 1042–1050.
[15] A.A. Edathil, P. Pal, F. Banat, Alginate clay hybrid composite adsorbents for the reclamation of industrial lean methyldiethanolamine solutions, Appl. Clay Sci., 156 (2018) 213–223.
[16] Q. Jin, P. Schexnailder, A.K. Gaharwar, G. Schmidt, Silicate cross-linked bionanocomposite hydrogels from PEO and chitosan, Macromol. Biosci., 9 (2009) 1028–1035.
[17] P. Li, N.H. Kim, Siddaramaiah, J.H. Lee, Swelling behavior of polyacrylamide/laponite clay nanocomposite hydrogels: pH-sensitive property, Composites, Part B, 40 (2009) 275–283.
[18] H.H. Bai, Q.S. Zhang, T. He, G. Zheng, G.Q. Zhang, L.B. Zheng, S.Q. Ma, Adsorption dynamics, diffusion and isotherm models of poly(NIPAm/LMSH) nanocomposite hydrogels for the removal of anionic dye Amaranth from an aqueous solution, Appl. Clay Sci., 124–125 (2016) 157–166.
[19] J. Wang, T.T. Xiao, R.Y. Bao, T. Li, Y.Q. Wang, D.X. Li, X.M. Li, T. He, Zwitterionic surface modification of forward osmosis membranes using N-aminoethyl piperazine propane sulfonate for grey water treatment, Process Saf. Environ., 116 (2018) 632–639.

[20] S. Liu, P.X. Wu, M.Q. Chen, L.F. Yu, C.X. Kang, N.W. Zhu, Z. Dang, Amphoteric modified vermiculites as adsorbents for enhancing removal of organic pollutants: bisphenol A and tetrabromobisphenol A, Environ. Pollut., 228 (2017) 277–286.
[21] Q.W. Lin, M.F. Gao, J.L. Chang, H.Z. Ma, Adsorption properties of crosslinking carboxymethyl cellulose grafting dimethyldiallylammonium chloride for cationic and anionic dyes, Carbohydr. Polym., 151 (2016) 283–294.
[22] X.D. Nie, A. Adalati, J. Du, H.H. Liu, S.M. Xu, J.D. Wang, Preparation of amphoteric nanocomposite hydrogels based on exfoliation of montmorillonite via in-situ intercalative polymerization of hydrophilic cationic and anionic monomers, Appl. Clay Sci., 97–98 (2014) 132–137.
[23] J.X. Zhu, P. Zhang, Y.H. Qing, K. Wen, X.L. Su, L.Y. Ma, J.M. Wei, H.M. Liu, H.P. He, Y. Xi, Novel intercalation mechanism of zwitterionic surfactant modified montmorillonites, Appl. Clay Sci., 141 (2017) 265–271.
[24] J.X. Zhu, Y.H. Qing, T. Wang, R.L. Zhu, J.M. Wei, Q. Tao, P. Yuan, H.P. He, Preparation and characterization of zwitterionic surfactant-modified montmorillonites, J. Colloid Interface Sci., 360 (2011) 386–392.
[25] H. Mittal, A. Maity, S.S. Ray, Gum karaya based hydrogel nanocomposites for the effective removal of cationic dyes from aqueous solutions, Appl. Surf. Sci., 364 (2016) 917–930.
[26] X. Zheng, D. Wu, T. Su, S. Bao, C. Liao, Q. Wang, Magnetic nanocomposite hydrogel prepared by ZnO-initiated photo-polymerization for La(III) adsorption, ACS Appl. Mater. Interfaces, 6 (2014) 19840–19849.
[27] L.Y. Ma, J.X. Zhu, Y.F. Xi, R.L. Zhu, H.P. He, X.L. Liang, G.A. Ayoko, Adsorption of phenol, phosphate and Cd(II) by inorganic–organic montmorillonites: a comparative study of single and multiple solute, Colloid Surf., A, 497 (2016) 63–71.
[28] X. Zhang, X. Shi, J. Chen, Y. Yang, G. Lu, The preparation of defective UiO-66 metal organic framework using MOF-5 as structural modifier with high sorption capacity for gaseous toluene, J. Environ. Chem. Eng., 7 (2019) 103405.
[29] J.F. Shen, N. Li, M.X. Ye, Preparation and characterization of dual-sensitive double network hydrogels with clay as a physical crosslinker, Appl. Clay Sci., 103 (2015) 40–45.
[30] C. Yu, X.Z. Tang, S.W. Liu, Y.L. Yang, X.C. Shen, C.C. Gao, Laponite crosslinked starch/polyvinyl alcohol hydrogels by freezing/thawing process and studying their cadmium ion absorption, Int. J. Biol. Macromol., 117 (2018) 1–6.
[31] P. Li, Siddaramaiah, N.H. Kim, S.-B. Heo, J.-H. Lee, Novel PAAm/Laponite clay nanocomposite hydrogels with improved cationic dye adsorption behavior, Composites, Part B, 39 (2008) 756–763.
[32] Q.Q. Zhong, Q.Y. Yue, B.Y. Gao, Q. Li, X. Xu, A novel amphoteric adsorbent derived from biomass materials: synthesis and adsorption for Cu(II)/Cr(VI) in single and binary systems, Chem. Eng. J., 229 (2013) 90–98.
[33] E. Oyervides-Muñoz, E. Pollet, G. Ulrich, G.J. Sosa-Santillán, L. Avérous, Original method for synthesis of chitosan-based antimicrobial agent by quaternary ammonium grafting, Carbohydr. Polym., 157 (2017) 1922–1932.
[34] Q.L. Lu, S.H. Zhang, M.C. Xiong, F.C. Lin, L.R. Tang, B. Huang, Y.D. Chen, One-pot construction of cellulose-gelatin supramolecular hydrogels with high strength and pH-responsive properties, Carbohydr. Polym., 196 (2018) 225–232.
[35] Y.B. Zhou, Y.H. Hu, W.W. Huang, G. Cheng, C.Z. Cui, J. Lu, A novel amphoteric β-cyclodextrin-based adsorbent for simultaneous removal of cationic/anionic dyes and bisphenol A, Chem. Eng. J., 341 (2018) 47–57.
[36] L.Y. Ma, Q.Z. Chen, J.X. Zhu, Y.F. Xi, H.P. He, R.L. Zhu, Q. Tao, G.A. Ayoko, Adsorption of phenol and Cu(II) onto cationic and zwitterionic surfactant modified montmorillonite in single and binary systems, Chem. Eng. J., 283 (2016) 880–888.
[37] F.L. Hu, K.M. Chen, H. Xu, H.C. Gu, Design and preparation of bi-functionalized short-chain modified zwitterionic nanoparticles, Acta Biomater., 72 (2018) 239–247.
[38] H.R. Kim, J.W. Jang, J.W. Park, Carboxymethyl chitosan-modified magnetic-cored dendrimer as an amphoteric adsorbent, J. Hazard. Mater., 317 (2016) 608–616.
[39] Q.P. Wu, R.R. You, Q.F. Lv, Y.L. Xu, W.J. You, Y. Yu, Efficient simultaneous removal of Cu(II) and $Cr_2O_7^{2-}$ from aqueous solution by a renewable amphoteric functionalized mesoporous silica, Chem. Eng. J., 281 (2015) 491–501.
[40] G.R. Mahdavinia, M. Soleymani, H. Etemadi, M. Sabzi, Z. Atlasi, Model protein BSA adsorption onto novel magnetic chitosan/PVA/laponite RD hydrogel nanocomposite beads, Int. J. Biol. Macromol., 107 (2018) 719–729.
[41] X.J. Huang, S.M. Xu, M. Zhong, J.D. Wang, S. Feng, R.F. Shi, Modification of Na-bentonite by polycations for fabrication of amphoteric semi-IPN nanocomposite hydrogels, Appl. Clay Sci., 42 (2009) 455–459.
[42] L.W. Zhao, Q. Li, X. Xu, W.J. Kong, X.D. Li, Y. Su, Q.Y. Yue, B.Y. Gao, A novel *Enteromorpha* based hydrogel optimized with Box–Behnken response surface emethod: synthesis, characterization and swelling behaviors, Chem. Eng. J., 287 (2016) 537–544.
[43] S.R. Shirsath, A.P. Hage, M. Zhou, S.H. Sonawane, M. Ashokkumar, Ultrasound assisted preparation of nanoclay Bentonite-FeCo nanocomposite hybrid hydrogel: a potential responsive sorbent for removal of organic pollutant from water, Desalination, 281 (2011) 429–437.
[44] B. Zhang, N. Chen, C.P. Feng, Z.Y. Zhang, Adsorption for phosphate by crosslinked/non-crosslinked-chitosan-Fe(III) complex sorbents: characteristic and mechanism, Chem. Eng. J., 353 (2018) 361–372.
[45] Sowmya, S. Meenakshi, Zr(IV) loaded cross-linked chitosan beads with enhanced surface area for the removal of nitrate and phosphate, Int. J. Biol. Macromol., 69 (2014) 336–343.
[46] K. Zhou, B.R. Wu, X.H. Dai, X.L. Chai, Development of polymeric iron/zirconium-pillared clinoptilolite for simultaneous removal of multiple inorganic contaminants from wastewater, Chem. Eng. J., 347 (2018) 819–827.
[47] S.X. Dong, Y.L. Wang, Y.W. Zhao, X.H. Zhou, H.L. Zheng, La^{3+}/$La(OH)_3$ loaded magnetic cationic hydrogel composites for phosphate removal: effect of lanthanum species and mechanistic study, Water Res., 126 (2017) 433–441.
[48] Y.A. Zheng, Y. Liu, A.Q. Wang, Fast removal of ammonium ion using a hydrogel optimized with response surface methodology, Chem. Eng. J., 171 (2011) 1201–1208.
[49] F. Wang, D. Liu, P.W. Zheng, X.F. Ma, Synthesis of rectorite/Fe_3O_4-CTAB composite for the removal of nitrate and phosphate from water, J. Ind. Eng. Chem., 41 (2016) 165–174.
[50] K. Didehban, M. Hayasi, F. Kermajani, Removal of anionic dyes from aqueous solutions using polyacrylamide and polyacrylic acid hydrogels, Korean J. Chem. Eng., 34 (2017) 1177–1186.
[51] Y. Yang, Z. Zheng, D. Zhang, X. Zhang, Response surface methodology directed adsorption of chlorate and chlorite onto MIEX resin and chemical properties study, Environ. Sci. Water Res. Technol., (2020), doi: 10.1039/C9EW01003C.
[52] Y.J. Liu, D.Y. Ying, L. Sanguansri, Y.X. Cai, X.Y. Le, Adsorption of catechin onto cellulose and its mechanism study: kinetic models, characterization and molecular simulation, Food Res. Int., 112 (2018) 225–232.
[53] K.N. Xu, F.Y. Lin, X.M. Dou, M. Zheng, W. Tan, C.W. Wang, Recovery of ammonium and phosphate from urine as value-added fertilizer using wood waste biochar loaded with magnesium oxides, J. Cleaner Prod., 187 (2018) 205–214.
[54] Y. Yang, M. Yang, Z. Zheng, X. Zhang, Highly effective adsorption removal of perfluorooctanoic acid (PFOA) from aqueous solution using calcined layer-like Mg-Al hydrotalcites nanosheets, Environ. Sci. Pollut. Res. Int., 27 (2020) 13396–13408.
[55] B. Hui, Y. Zhang, L. Ye, Preparation of PVA hydrogel beads and adsorption mechanism for advanced phosphate removal, Chem. Eng. J., 235 (2014) 207–214.
[56] E. Gamshadzehi, M. Nassiri, H. Ershadifar, One-pot synthesis of microporous Fe_2O_3/g-C_3N_4 and its application for efficient removal of phosphate from sewage and polluted seawater, Colloid Surf., A, 567 (2019) 7–15.
[57] J.R. Li, F.K. Wang, H. Xiao, L. Xu, M.L. Fu, Layered chalcogenide modified by lanthanum, calcium and magnesium for the removal of phosphate from water, Colloid Surf., A, 560 (2019) 306–314.

[58] R. Li, J.J. Wang, B. Zhou, Z. Zhang, S. Liu, S. Lei, R. Xiao, Simultaneous capture removal of phosphate, ammonium and organic substances by MgO impregnated biochar and its potential use in swine wastewater treatment, J. Cleaner Prod., 147 (2017) 96–107.
[59] H.X. Huo, H. Lin, Y.B. Dong, H. Cheng, H. Wang, L.X. Cao, Ammonia-nitrogen and phosphates sorption from simulated reclaimed waters by modified clinoptilolite, J. Hazard. Mater., 229–230 (2012) 292–297.
[60] P. Xia, X.J. Wang, X. Wang, J.K. Song, H. Wang, J. Zhang, J.F. Zhao, Struvite crystallization combined adsorption of phosphate and ammonium from aqueous solutions by mesoporous MgO loaded diatomite, Colloid Surf., A, 506 (2016) 220–227.
[61] Y.Y. Zhou, X.C. Liu, L. Tang, F.F. Zhang, G.M. Zeng, X.Q. Peng, L. Luo, Y.C. Deng, Y. Pang, J.C. Zhang, Insight into highly efficient co-removal of p-nitrophenol and lead by nitrogen-functionalized magnetic ordered mesoporous carbon: performance and modelling, J. Hazard. Mater., 333 (2017) 80–87.